ACCSCIENCE PUBLISHING

Journal of Seismic Exploration

ARTICLE

Inversion model combination for microseismic source positioning with Multi-Objective Grasshopper Optimization Algorithm

Cong Pang[1,2], Tianwen Zhao[3], Guoqing Chen[4,5], Sirui Liu[1], Xingxing Li[1], Ya Xiang[1], and Piyapatr Busababodhin[5]*

[1]Institute of Seismology, China Earthquake Administration, Wuhan, Hubei, China

[2]Wuhan Gravitation and Solid Earth Tides, National Observation and Research Station, Wuhan, Hubei, China

[3]Department of Trade and Logistics, Daegu Catholic University, Gyeongsan, Daegu, Republic of Korea

[4]Mathematical Modeling Research Center, Chengdu Jincheng College, Chengdu, Sichuan, China

[5]Department of Mathematics, Faculty of Science, Mahasarakham University, Kantharawichai, Maha Sarakham, Thailand

Abstract

The precise determination of microseismic source locations is one of the core components of theoretical research in microseismic monitoring technology. Multi-objective intelligent optimization is an effective approach for microseismic source positioning, but it faces challenges such as unclear rationality of model combinations, susceptibility to local optima, and significant variability in positioning results. To address these issues, four distinct mathematical models for microseismic source positioning were designed based on the arrival time difference model and the arrival time difference quotient model. These models were then combined in pairs to form six different microseismic source positioning model combinations, which were used as the optimization objective functions for the multi-objective computational algorithm. A set of microseismic source forward modeling experiments based on three-dimensional polyhedral array shapes, two sets of engineering microseismic data validation experiments, and one set of multi-objective computational method comparison experiments were designed. the multi-objective grasshopper optimization algorithm (MOGOA) was introduced to solve the six model combinations and employed in four sets of microseismic source positioning experiments. Multiple statistical metrics were applied to evaluate the performance of each model combination. The experimental results indicate that the microseismic inversion mathematical model combination (TDA, TDA-P1), combined with the MOGOA algorithm's multi-objective optimization positioning strategy, can achieve high microseismic source positioning accuracy under relatively reliable microseismic event data, and the model calculations are relatively robust. Under microseismic blasting data, the average positioning error over 100 rounds reached 27.6035 m, with standard deviation and interquartile range averages of only 3.2114 m and 5.5896 m, respectively, outperforming other inversion model combinations and similar multi-objective positioning methods. For microseismic event data with significant

***Corresponding author:**
Piyapatr Busababodhin
(piyapatr.b@msu.ac.th)

Citation: Pang C, Zhao T, Chen G, *et al*. Inversion model combination for microseismic source positioning with Multi-Objective Grasshopper Optimization Algorithm. *J Seismic Explor*. 2026;35(1):151-170.
doi: 10.36922/JSE025420089

Received: October 13, 2025

Revised: November 26, 2025

Accepted: December 1, 2025

Published online: January 14, 2026

Copyright: © 2026 Author(s). This is an Open-Access article distributed under the terms of the Creative Commons Attribution License, permitting distribution, and reproduction in any medium, provided the original work is properly cited.

Publisher's Note: AccScience Publishing remains neutral with regard to jurisdictional claims in published maps and institutional affiliations.

systematic errors, the microseismic inversion mathematical model combination (TDA-P1, TDQA-P1) demonstrates superior positioning performance, with an average positioning error of 151.1915 m over 100 iterations, significantly outperforming other model combinations. These model combination positioning performance studies hold practical application value in the field of microseismic monitoring.

Keywords: Microseismic source positioning; Multi-objective optimization; Combination of inversion mathematical models; Time difference quotient of arrival; Time difference of arrival; Multi-Objective Grasshopper Optimization Algorithm

1. Introduction

Microseismic source positioning is a core component of microseismic monitoring technology, crucial for geological disaster early warning, mine safety monitoring, and structural stability assessment. Inverse mathematical models and their solution methods are key components of microseismic source location research. The rational selection and combination of mathematical models is an effective approach to improving positioning accuracy and stability.[1-9] Traditional mathematical models for positioning primarily include travel time (TT) models, time difference of arrival (TDA) models, distance difference models, and time difference quotient models. Such as the TDA model, derived from the TT functions of two different points in the same array, eliminates the P-wave first arrival time parameter and can represent the deviation between observed and theoretical arrival time differences. While offering advantages such as physical intuition and rapid convergence, these methods and their direct variants are extremely sensitive to velocity model anomalies, resulting in potentially sudden increases in location errors and instability. To overcome this limitation, researchers have developed models such as the time difference quotient of arrival (TDQA). These mathematically eliminate two physical parameters, wave velocity and first wave arrival time, and can represent the consistency of wave velocity factors within a region. This theoretical advantage eliminates the need for prior velocity measurements, thus reducing the complexity of solving the inversion model. However, this can also be affected by errors in microseismic event arrival time data.[10,11] Combining multiple inversion mathematical models or balancing their characteristics can effectively circumvent the drawbacks of a single model—TDA relies on precise wave velocity, while TDQA requires no prior velocity measurements (suitable for homogeneous media). Optimizing multiple fitness functions to find the optimal location is a worthy microseismic source positioning strategy. To enrich our sample of inversion mathematical models, this paper adds constant offset terms (such as addition and subtraction of 1) to the TDA and TDQA models. This approach, by amplifying the arrival time difference constants, avoids premature iteration termination. This approach offers a promising avenue for inversion model improvement, ultimately resulting in the development of multiple inversion mathematical model examples.

Multi-objective optimization is an important method for simultaneously optimizing multiple inversion mathematical models. Evolving primarily from single-objective optimization algorithms, it can simultaneously handle two or more multivariable objective functions.[12-14] With the continuous advancement of heuristic algorithms, swarm intelligence optimization algorithms, due to their global search capabilities and advantages in nonlinear processing, have gradually become the mainstream method for optimizing earthquake source positioning models. New biomimetic optimization algorithms, such as the Grey Wolf Optimizer,[15,16] the Whale Optimization Algorithm,[17,18] and the Ant Lion Optimization,[19,20] have demonstrated significant potential in solving high-dimensional non-convex optimization problems by simulating the behavior of biological swarms in nature. Compared with traditional linear model solving methods (such as Geiger iteration method), these algorithms have three major advantages: (i) Strong robustness: insensitive to initial value selection and noise interference; (ii) high convergence: avoid premature convergence and effectively jump out of local extreme values; (iii) parallel mechanism: adapt to the needs of multi-parameter joint inversion. Multi-objective optimization provides a new idea for earthquake source positioning by integrating multiple complementary objective functions. Its core lies in constructing a Pareto optimal solution set and balancing the constraints of different mathematical models. Based on the new single-objective group optimization algorithm, a multi-objective optimization algorithm is formed, which can further improve the accuracy and stability of microseismic source positioning.

To address the above challenges, this paper proposes an innovative research framework of multi-objective

grasshopper optimization algorithm (MOGOA)[21-26] and inversion mathematical model combination (TDA, TDQA, and its variants). Its theoretical breakthroughs are reflected in three aspects: (i) *Multi-objective collaborative mechanism:* constructing six groups of dual-objective optimization models consisting of any two inversion mathematical models of TDA, TDQA and its variants to form optimization objectives with complementary physical meanings. (ii) *Algorithm-model coupling design:* The multi-objective extension of the grasshopper optimization algorithm (MOGOA) is introduced to give full play to its advantages in global search mechanism and adaptive step size adjustment, overcoming the shortcomings of other similar algorithms in the uniformity of Pareto front distribution. (iii) *Multi-group positioning experiment design:* Combining a set of simulated cube sensor array microseismic event forward data and two sets of engineering microseismic event data, a microseismic source positioning comparison experiment based on the MOGOA model and six sets of mathematical models is designed; finally, the Second-Generation Non-Dominated Sorting Genetic Algorithm (NSGA-II)[27-29] and the multi-objective particle swarm optimization algorithm (MOPSO)[28-30] are introduced as the comparison algorithms for solving the multi-objective optimization model of MOGOA.

In summary, the microseismic source positioning method proposed in this study, which combines multi-objective optimization with inversion models, offers a systematic and robust framework to address the two major challenges faced by traditional approaches: model uncertainty and data error. First, unlike traditional methods that rely on a single physical model, this study employs a multi-model fusion strategy to leverage the complementary nature of different objective functions in physical terms. When velocity models contain errors, objective functions sensitive to absolute TTs may conflict with those sensitive to geometric relationships. Our approach automatically achieves an optimal trade-off between these competing objectives by seeking Pareto optimal solutions, significantly enhancing the robustness of positioning results against model mismatches. When confronted with noisy initial-arrival data, this framework adaptively balances the susceptibility of different objective functions to errors without requiring predefined complex weighting schemes. This demonstrates greater intelligence and adaptability compared to traditional weighted least squares methods. Finally, although intelligent optimization algorithms are computationally more complex than least squares, their robust global search capability is essential for handling complex objective function spaces with multiple local minima caused by real-world errors. As demonstrated by parameter analysis, our method exhibits insensitivity to parameter variations after reaching performance thresholds, proving its convenience and stability in practical applications. Therefore, the value of this research lies not in negating traditional methods, but in providing a new and effective technical pathway for high-reliability microseismic positioning in complex, non-ideal engineering environments.

2. Combination of mathematical models for microseismic source positioning

The accurate selection of mathematical models is a key factor in implementing multi-target high-precision positioning. Classical mathematical models for microseismic source positioning can be divided into TT models, arrival time difference models, arrival time difference quotient models, or arrival distance difference models. There are many cases of research on single models. Here, we will combine the time difference model and the arrival time difference quotient model to study the combined model and formulate a mathematical model combination plan based on this. The basic mathematical formula for microseismic source positioning is:

$$l_i = \sqrt{\left(x_i - x_0\right)^2 + \left(y_i - y_0\right)^2 + \left(z_i - z_0\right)^2} \tag{1}$$

$$l_i = v \cdot \left(t_i - t_0\right) \tag{2}$$

$$T_k = t_i - t_j, i \neq j \tag{3}$$

$$L_k = l_i - l_j = v \cdot T_k, i \neq j \tag{4}$$

where l_i is the spatial distance from the i-th seismic pickup (x_i, y_i, z_i) to the microseismic source (x_0, y_0, z_0), $i = 1,2,\ldots,m$; m is the number of seismic pickups receiving valid seismic wave signals; v is the seismic wave velocity, in this case the P-wave velocity; and t_0 is the time of the artificial explosion or microseismic event.

T_k is defined as the difference in arrival time of the seismic waves recorded by two seismic pickups, $T_k = t_i - t_j$, with $i \neq j$; L_k is defined as the difference in spatial distance between the two seismic pickups and the microseismic source, $L_k = l_i - l_j = v.T_k$ Based on the definitions of the above key parameters, the following four mathematical models for microseismic source positioning with different meanings are established:

$$f_1 = \sum_{k=1}^{N} \left(T_k - \frac{L_k}{v} \right)^2 \tag{5}$$

$$f_2 = \sum_{k=1}^{N} \left| \left(T_k - \frac{L_k}{v} \right) + 1 \right|^2 - 1 \tag{6}$$

$$f_3 = \sum_{p,q=1;p>q}^{M} \left(\frac{T_p}{L_p} - \frac{T_q}{L_q} \right)^2 \tag{7}$$

$$f_4 = \sum_{p,q=1;p>q}^{M} \left| \left| \frac{T_p}{L_p} - \frac{T_q}{L_q} + 1 \right|^2 - 1 \right| \tag{8}$$

In the above formulas, f_1 is the classic arrival time difference model, which reflects the degree of deviation between the observed arrival time difference and the theoretical arrival time difference, denoted as TDA; f_2 is based on f_1, adding 1 to the arithmetic square method and then subtracting 1 from the square method as a whole to obtain the absolute value. This deformation can amplify the amplitude of the time difference deviation value, avoiding the premature termination of the iteration in the model solution, and is also conducive to the algorithm to find a more appropriate local optimal solution, making the calculation result more credible, denoted as TDA-P1; f_3 is the classic arrival time difference quotient model The inverse form of the model takes the observed time difference as the numerator of the sub-item and the theoretical arrival distance as the denominator. It contains the seismic wave arrival time information of 3 or 4 seismic pickups, reflecting the degree of difference between the two observed wave velocity factors ($\gamma_p = 1/v_p$ and $\gamma_q = 1/v_q$) calculated using different seismic pickup combinations, denoted as TDQA. This model does not require advanced velocity measurement and is suitable for homogeneous medium environment; f_4 is a new model that is deformed based on f_3. The principle is the same as f_2, denoted as TDQA-P1.

3. Multi-Objective Grasshopper Optimization Algorithm

3.1. Standard grasshopper optimization algorithm

The grasshopper optimization algorithm (GOA) proposed in 2017 is a new bionic optimization algorithm that mimics the cohabitation and migration of grasshopper larvae and adults. It takes advantage of the differentiated biological characteristics of grasshopper larvae, which are slow to move, and adults, which are fast to move. That is, grasshoppers move slowly in the larval stage and only move within a small range, while adults have strong hind legs and are good at long-distance jumping and moving quickly. This biological learning ability helps to carry out local search and global optimization at the same time. The change of grasshopper position is subject to the interaction force, gravity and wind force in the natural environment. Therefore, the GOA model calculates the position of the i-th grasshopper at the t+1th iteration as follows:

$$X_i = S_i + G_i + A_i \tag{9}$$

In **Formula 9**, X_i is the position of the i-th grasshopper, S_i is the interaction between the i-th grasshopper and other grasshoppers, G_i is the gravity acting on the i-th grasshopper, and A_i is the wind force acting on the i-th grasshopper.

$$S_i = \sum_{j=1}^{N} s d_{ij} \breve{d}_{ij} \tag{10}$$

In **Formula 10**, N is the number of grasshopper populations, d_{ij} is the absolute distance between grasshopper i and grasshopper j; $\breve{d}_{ij}$ is the unit vector of the distance between grasshopper i and grasshopper j.

$$s(r) = f e^{-\frac{r}{l}} - e^{-r} \tag{11}$$

In **Formula 11**, f is the attraction strength; l is the attraction range; and S(.) represents the interaction force function between grasshopper i and grasshopper j. Grasshopper experience both repulsive and attractive forces. When they are too close, repulsion occurs, whereas when they are too far, attraction arises. The area where reLocust's and attraction are balanced is called the comfort zone. Repulsion can prevent the algorithm from converging prematurely, ensuring effective exploration.

$$G_i = -g \breve{e}_g \tag{12}$$

In **Formula 12**, g is the gravitational acceleration constant; $\breve{e}_g$ is the unit vector pointing to the center of the Earth.

$$A_i = u \breve{e}_W \tag{13}$$

In **Formula 13**, u is the drift constant; and $\breve{e}_W$ is the unit vector of the wind direction. Because this will cause the grasshoppers to quickly reach their comfort zone and the swarm will not converge to a specific location, this mathematical model cannot be directly used to solve the optimization problem. Ultimately, it is necessary to ignore the influence of gravity and ensure that the direction of the wind force is always toward the optimal grasshopper position. The final formula for updating the grasshopper position using the GOA model is:

$$x_{i,d}(t+1) = c \left(\sum_{j=l,j\neq i}^{N} c \frac{ub_d - lb_d}{2} s(|x_{j,d}(t) - x_{i,d}(t)|) \frac{x_{j,d}(t) - x_{i,d}(t)}{d_{ij}(t)} \right) + T_d' \tag{14}$$

In **Formula 14**, $x_{i,d}(t)$ is the coordinate value of the grasshopper individual in the d-th dimension of the position vector at the t-th iteration; c is the linear dynamic attenuation coefficient related to the maximum number of iterations, which affects the grasshopper's global optimization or local search ability; ub_d and lb_d are the upper and lower limit thresholds on the d-th dimension of the grasshopper individual position, respectively; S(.) represents the interaction force function of grasshopper i affected by grasshopper j; d_{ij} is the absolute distance between grasshopper i and grasshopper j; and $T_d^{'}$ is the coordinate value of the d-th dimension of the optimal position vector previously obtained by the grasshopper colony.

3.2. MOGOA

MOGOA is a multi-objective intelligent bionic algorithm that simulates the differentiated behavioral activities of locusts across different life stages. Its core concept involves utilizing long-distance migrating adult locusts to search the global space, while crawling, feeding nymphs explore the local space. The hunting actions of individual locusts depend on the combined effects of intra-population forces, gravity, and wind force. Optimal solutions are selected through Pareto dominance and crowding distance mechanisms. Key differences between MOGOA and standard GOA include:

(i) *Pareto dominance mechanism:* Unlike single-objective methods that directly compare fitness values, in multi-objective optimization we employ the concept of "Pareto dominance" to evaluate solutions. After population initialization and during each iteration, we assess the quality of all locusts (solutions) using Pareto dominance relations. A solution not dominated by any other solution in the population is termed a non-dominated solution. The collective set of all non-dominated solutions forms the Pareto frontier for that iteration.

(ii) *External archive maintenance:* Since multi-objective optimization yields a set of solutions (the Pareto optimal solution set), a dedicated container is required to store high-quality non-dominated solutions discovered during iterations. This container is termed the external archive. During algorithm execution, newly discovered non-dominated solutions are continuously compared against existing solutions in the archive. Based on the Pareto dominance relationship, old solutions dominated by new ones are removed from the archive, while new solutions not dominated by any existing solution are added.

(iii) *Diversity preservation strategy (archive maintenance and leader selection):* This constitutes the most critical component of MOGOA, ensuring that the final Pareto solution set not only approximates the true frontier but also uniformly covers the entire frontier with excellent distribution. First, when the external archive is full and solutions must be removed, we employ "crowding distance" as the metric. This distance measures how densely a solution is surrounded by neighboring solutions in the objective space. A solution with a larger crowding distance indicates sparser surrounding solutions, making it more crucial for maintaining frontier diversity. Second, MOGOA avoids a single global optimum by selecting a "leader" from the external archive. We employ a roulette wheel selection method where the selection probability is proportional to the solution's crowding distance—solutions with higher crowding distances have a greater chance of being chosen as leaders. This mechanism encourages the locust population to migrate toward the sparsest and least explored regions of the current Pareto frontier. It effectively balances exploitation (searching within known high-quality regions) and exploration (seeking new potential solutions), serving as the core driver for maintaining diversity within the solution set.

Multi-objective positioning calculations generally use two or more inversion mathematical models to construct different fitness functions. The dependent variable of each function has zero as its theoretical minimum value, and the independent variables are the parameters to be solved in the inversion model, which can be P-wave velocity, approximate three-dimensional coordinates, or the time of microseismic occurrence. The known parameters are the three-dimensional coordinates of the microseismic array measurement points, the true microseismic source location, and the first arrival time of the seismic wave. The solution model for multi-objective optimization problems is generally as follows:

$$minF = \left\{ f_m, f_n \right\} \tag{15}$$

In **Formula 15**, m=1,2,3,4, n=1,2,3,4,$m \neq n$.

Different sources of model combinations directly impact the effectiveness of microseismic source positioning. For instance, the TDA model is sensitive to absolute timing errors but provides better distance constraints; conversely, the TDQA model is insensitive to absolute timing errors and wave velocity because it represents a ratio, yet offers superior directional constraints. Therefore, combining these two distinct model types theoretically achieves complementary distance and direction constraints. This enables more robust solutions than single models or same-type combinations when initial arrival picking

errors (affecting TDA) or inaccurate velocity models (impacting both) occur. To test the actual positioning effectiveness of different model combinations, the four standalone inversion mathematical models mentioned in section 1 were paired to construct six combination models with significantly different physical meanings:

(i) *MO-1:* Combines the TDA Model f_1 with the TDA-P1 model f_2. This pair exhibits smoothing effects on pure random noise but may "disagree" under strong systematic errors, as one minimizes residuals while the other biases them, leading to Pareto frontier divergence or convergence failure. Its performance typically falls short of combinations with complementary models.

(ii) *MO-2:* Combines the TDA model f_1 with the TDQA model f_3. When velocity models exhibit global scaling errors or systematic bias in first-arrival picking, f_1 may fail while f_3 maintains stable geometric constraints. Together, even with minor absolute positional shifts, their relative geometric shapes can "pull" the source back into the correct region, demonstrating exceptional robustness.

(iii) *MO-3:* Combines the TDA model f_1 with the TDQA-P1 model f_4. Building upon the advantages of the f_1& f_3 combination, it further enhances resistance to complex error patterns where "the theoretical TTs at all stations are systematically overestimated or underestimated." This is theoretically a more robust combination, though it may require additional iterations to balance the two objectives.

(iv) *MO-4:* Combines the TDA-P1 model f_2 with the TDQA model f_3. This combination is highly suitable for addressing scenarios with overall first-arrival time shifts (constant delays caused by picker algorithms). f_2 compensates for this overall shift, while f_3 ensures correct geometry. It may perform exceptionally well when processing noisy data with constant bias.

(v) *MO-5:* Combination of the TDA-P1 model f_2 and the TDQA-P1 model f_4. This is theoretically the most "aggressive" compensation combination. It may demonstrate unique advantages when complex absolute and relative systematic errors coexist in the data; however, it may also introduce instability due to over-compensation, with its performance highly dependent on the actual error distribution.

(vi) *MO-6:* Combines the TDQA model f_3 with the TDQA-P1 model f_4. Similar to the f_1& f_2 combination, this pair primarily smooths random noise in the relative residual domain. Both are highly insensitive to overall scaling errors in the velocity model but may sacrifice absolute positioning accuracy. Their combination allows fine-tuning within the constraints of relative geometry.

4. Forward and inversion simulation experiments of microseismic sources

To verify the theoretical effectiveness of the six positioning mathematical model combinations and the MOGOA for microseismic source positioning, a set of forward and inversion simulation experiments were designed. Three-dimensional polyhedron array data simulation and first-wave arrival time calculations were performed on MATLAB 2024b and Windows 10 64-bit systems. The MOGOA algorithm uses the following preset parameters: 20 search agents (populations), 200 maximum iterations, 3 search target dimensions, 40 grasshopper populations, a lower search limit of (0 0 0), an upper search limit of (5000 5000 5000), and 100 positioning experiment cycles. In this experiment, the seismic wave (P-wave) propagation speed in the medium is set to 2500 m/s. The earthquake took place on August 10, 2025, at 14:19:00. The earthquake location coordinates are uniformly set to (655.1, 349.7, 187.2). The microseismic monitoring array is a three-dimensional polyhedron (approximately spherical), with 12 detectors evenly distributed on its boundary. The relevant simulation data are shown in Figure 1 and Table 1.

Figure 1 presents simulated data from a microseismic monitoring network based on a polyhedral array, comprising 12 three-dimensional monitoring points (blue markers) and one real seismic source (red marker). Based on the coordinates of the monitoring points, wave velocities, and the location of the seismic source, the first-arrival times of seismic waves from the real source to each monitoring point can be calculated in seconds, as detailed in Table 1.

Table 1 presents the three coordinate values and first-arrival times for 12 monitoring stations. It is evident that

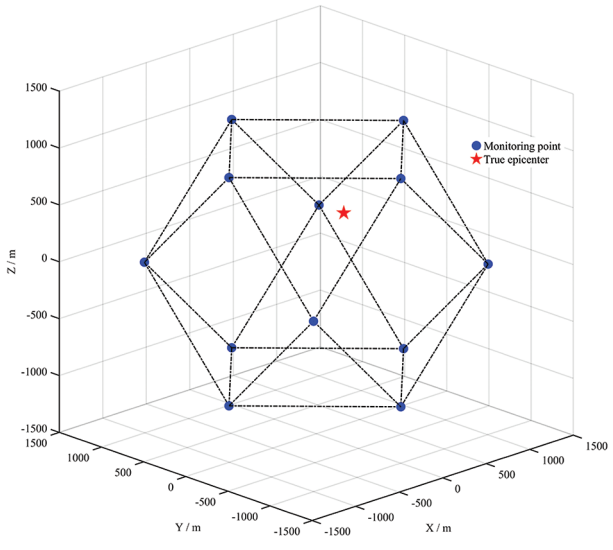

Figure 1. Sensor's network layout for simulation experiment

Table 1. Simulation data of microseismic source forward modeling

Serial number	Vibration pickup coordinates (m)			By then (s)
	x	*y*	*z*	
1	1003.213 6	1003.551 3	0.074 2	0.3056
2	1003.153 4	−1003.716 0	0.016 4	0.5639
3	−1003.345 8	1003.234 8	0.305 5	0.7169
4	−1003.168 9	−1003.190 5	0.215 3	0.8593
5	0.156 3	1003.142 1	1003.410 8	0.4934
6	0.138 7	1003.035 6	−1003.307 7	0.6030
7	0.069 8	−1003.018 7	1003.053 9	0.6840
8	0.043 2	−1003.062 9	−1003.071 2	0.7668
9	1003.356 7	0.110 2	1003.158 1	0.3814
10	1003.154 7	0.085 6	−1003.104 6	0.5153
11	−1003.286 5	0.041 7	1003.093 5	0.7524
12	−1003.137 4	0.017 4	−1003.410 7	0.8285

each coordinate value possesses four distinct significant digits after the decimal point. This feature enhances the model's physical realism and generalization capability, prevents numerical computation from exhibiting linear correlation, and consequently improves the performance and robustness of the optimization algorithm.

Figure 2 shows a box plot of the microseismic source positioning results based on MOGOA and different inversion model combinations. The upper and lower boundary lines of the box in the figure indicate the upper quartile (Q3) and lower quartile (Q1) of the positioning results, respectively. The solid line inside the box represents the median of the positioning result. The red triangle marks the data identified as outliers by the box plot. The upper and lower solid horizontal lines outside the box represent the maximum and minimum values, respectively. Table 2 shows the statistics of the microseismic source positioning results based on different inversion model combinations based on three-dimensional polyhedron array simulation and the MOGOA model. The indicators Mean, IQR, STD, Best, Worst, Duration, Fit-1, and Fit-2 represent the mean, interquartile range (IQR), standard deviation (STD), minimum and maximum of the location error dataset, the average calculated time for positioning, the final fitness function mean of Model 1 (the first submodel from the left in the combination model), and the final fitness function mean of Model 2, respectively.

From Figure 2 and Table 2, we can see that:

(i) The overall positioning accuracy and robustness of the MO-6 combination model are far inferior to those of other inversion mathematical models. The order of positioning accuracy is MO-1 > MO-3 > MO-5 > MO-4 > MO-2 > MO-6. The positioning means value of the 100-round combination of models TDA-P1 and TDA reached 0.0041 m, with the highest positioning accuracy. Its performance in the indicators IQR (0.0014 m) and STD (0.0082 m) was also the most significant, proving that the solution process of the MO-1 combination is not only more accurate but also relatively more robust. The positioning results do not have a large error in the source approximate solution.

(ii) The positioning effects of the combinations MO-2, MO-3, MO-4, and MO-5 are generally comparable. The meaning of their 100-round positioning errors is all between 0.12 and 0.19m, and the STD values are all within 0.30 m or less, indicating that the positioning effect of the above four model combinations is also high, and they can be used as alternatives or substitutes for the MO-1 combination model. The specific actual positioning reliability and accuracy differences need to be further explored in combination with other experiments.

(iii) From the fitness function value indicators (Fit 1, Fit-2), the main reason for the poor statistical

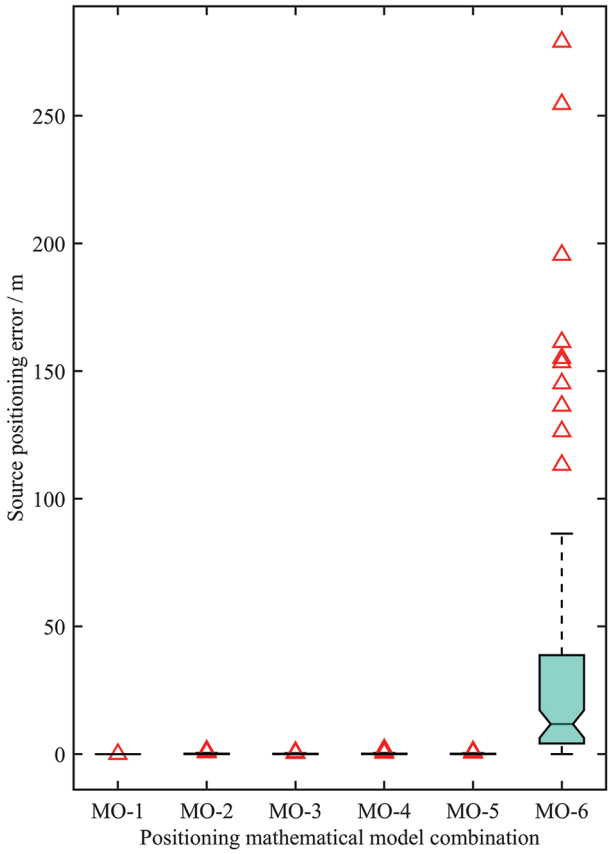

Figure 2. Box plot of microseismic source positioning results based on Multi-Objective Grasshopper Optimization Algorithm (MOGOA) and different inversion model combinations

Table 2. Statistics results of microseismic source positioning based on different inversion model combinations using three-dimensional polyhedral array simulation and the MOGOA model

Combination	Model 1	Model 2	Statistical values of microseismic source positioning results							
			Mean (m)	STD (m)	IQR (m)	Best (m)	Worst (m)	Duration (s)	Fit-1	Fit-2
MO-1	TDA	TDA-P1	0.0041	0.0082	0.0014	8.0419e-05	0.0443	2.8347	4.8969e-10	0.0001
MO-2	TDA	TDQA	0.1834	0.2758	0.1898	0.0002	1.3571	3.6136	6.1683e-07	4.6337e-11
MO-3	TDA	TDQA-P1	0.1236	0.1626	0.1427	0.0003	0.8512	3.5736	2.3508e-07	0.0001
MO-4	TDA-P1	TDQA	0.1706	0.2806	0.1775	0.0004	1.8587	3.6350	0.0054	3.5629e-11
MO-5	TDA-P1	TDQA-P1	0.1432	0.2118	0.1666	0.0004	1.0701	3.6471	0.0045	0.0001
MO-6	TDQA	TDQA-P1	34.5344	53.0555	34.5673	0.0238	278.98099	4.5234	7.0563e-08	0.0110

Abbreviations: IQR: Interquartile range; MOGOA: Multi-Objective Grasshopper Optimization Algorithm; STD: Standard deviation; TDA: Time difference of arrival; TDQA: Time difference quotient of arrival.

positioning accuracy and insufficient robustness of the combination MO-6 in 100 rounds of experiments is that the optimization effect of the TDQA-P1 model is not ideal (its Fit-2 value is 0.0001, which is more than 100 times different from the Fit-2 values of other combination models, while Fit-1 is not much different from other combination models). This is related to its theoretical design of eliminating wave speed as one of the independent variables of the fitness function, which makes it lose sufficient physical constraints in the process of determining the approximate solution and fall into the local optimum. At the same time, the design method of adding 1 in the TDQA-P1 mathematical model exacerbates this phenomenon.

After reviewing the statistical data from 100 rounds of microseismic source positioning results, we proceeded to present and analyze the specific variations in each round's positioning outcomes. This enables a dissection of the oscillation patterns of the error curves for each combined model. Figure 3 is a graph showing the microseismic source positioning results of 100 rounds and six combination models based on polyhedron array simulation. Figure 4 shows the local approximate dissolution points of six microseismic source positioning combination models based on polyhedron array simulation and the MOGOA model.

From Figures 3 and 4, we can see that:

(i) For a single combination model, the number of abnormal approximate solutions with large positioning errors is small compared to the total approximate solution samples. Many sources' approximate solutions are mainly concentrated near the true source location (655.1, 349.7, 187.2). Among them, the approximate solution set of MO-1 is more concentrated, almost coinciding with the true source location and being covered by many scattered points.

(ii) As shown in Figure 4, the number of approximate solutions between the lower limit (654, 349, 186.5) and the upper limit (656, 350, 187.5) of the spatial coordinates of the MO-6 combination is very small and presents a divergent distribution phenomenon. Many approximate solutions have positioning errors distributed between 0 and 50 m. The positioning errors of most source approximate solutions of other combination models are below 0.5 m.

The successful execution of microseismic source forward modeling simulations alone is insufficient to demonstrate the reliability of multi-objective positioning models. Further validation using microseismic event data from real-world engineering cases is necessary to achieve a closed-loop verification process integrating simulation with empirical testing.

5. Engineering verification

5.1. Microseismic experiment of a deep mining mine

The validation was conducted using microseismic experimental data from a deep mining mine in China. A total of 12 microseismic monitoring units were installed in the mine. The artificial blasting locations were (3500.0, 3520.5, 102.0), the detonation time was 00:00, and the explosive charge was 2.25 kg. After the successful blast, nine P-wave arrival times were observed, denoted as T1 to T12, as shown in Table 3. The experimental simulation used MATLAB 2024B data processing tools and the corresponding standard function toolbox. The MOGOA algorithm uses the following preset parameters: 40 swarm search agents, 200 maximum iterations, 3 search target dimensions, a lower search limit of (0, 0, 0), an upper search limit of (5000, 5000, 5000), and 100 positioning experiment cycles.

Table 4 shows the statistical results of the calculation of six combined models for microseismic source positioning

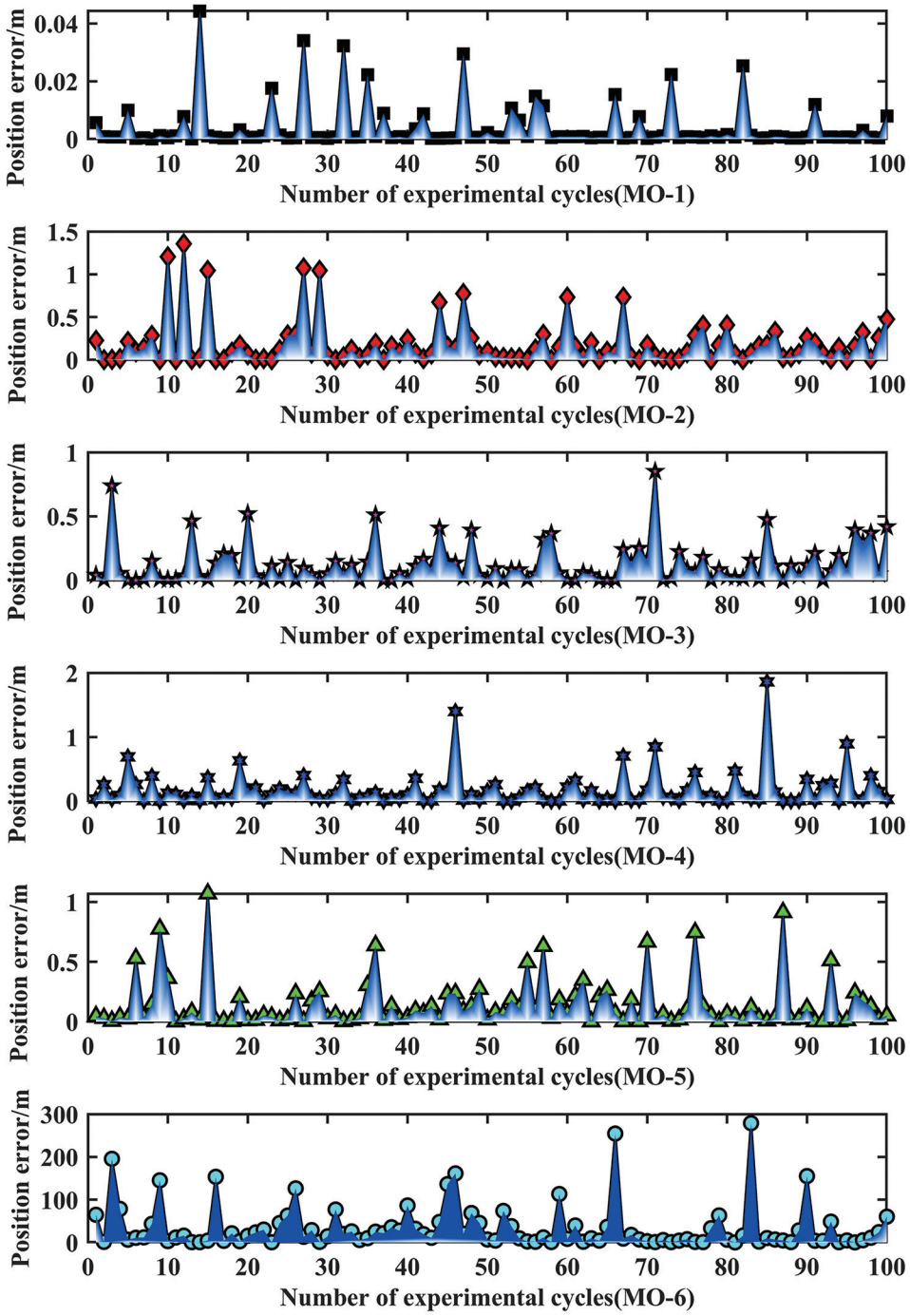

Figure 3. Position-error curves for six microseismic source positioning combination models (MO-1 to MO-6), obtained from 100 rounds of polyhedral-array simulations

based on the MOGOA model and deep mining microseismic events. The indicators Mean, IQR, STD, Best, Worst, Duration, Fit-1, and Fit-2 represent the mean, IQR, STD, minimum and maximum values of the positioning error dataset, the average positioning calculation time, the final fitness function mean of Model 1 (the first submodel from the left in the combined model), and the final fitness function mean of Model 2, respectively. Figure 5 shows a box plot of the calculation results of six combined models for microseismic source positioning based on the MOGOA model and deep mining microseismic events. The upper and lower boundary lines of the boxes in the

figure represent the upper quartile (Q3) and lower quartile (Q1) of the positioning results, respectively. The solid line inside the box represents the median of the positioning result. Red triangles mark data identified as outliers by the box plot. The upper and lower solid horizontal lines outside the box represent the maximum and minimum values, respectively.

From Figure 5 and Table 4, we can see that:

(i) The overall positioning accuracy and robustness of the MO-6, MO-2, and MO-3 combination models are far inferior to those of other inversion mathematical models. They are more sensitive to the noise or error of microseismic data, which seriously restricts the global search ability of the optimization model. The order of positioning accuracy is MO-5 > MO-4 > MO-1 > MO-3 > MO-2 > MO-6. The 100-round combination positioning mean value of the model TDA-P1 and TDQA-P1 combination reached 151.1915 m, which is the highest positioning accuracy. It also performs best in terms of the indicators IQR (121.9566 m) and STD (66.5852 m). This proves that the MO-5 combination is not only more accurate but also more robust in solving real engineering blasting data. The positioning results do not have excessive errors or are judged as abnormal values by the box plot.

(ii) The positioning effects of the MO-1 and MO-4 combinations are similar overall. The mean values of their 100-round positioning errors are both between 700 and 800 m, and the STD values are also around 1000 m. However, the IQR index of MO-4 (139.1974 m) is significantly better than that of MO-1 (981.4611 m), indicating that the comprehensive positioning effect of the MO-4 combination over 100 rounds is only

Table 3. Microseismic experimental data from SBKC mine

Detector	Vibration pickup coordinates (m)			By then (ms)
	x	*y*	*z*	
T1	4088.2	3548.6	61.6	1093.1
T2	4413.1	3057.4	−2.2	1419.0
T3	4798.0	2904.0	−52.4	1304.1
T4	4280.9	2834.0	−83.9	1224.8
T5	4569.8	2183.0	−199.3	1392.1
T6	3978.4	3774.3	151.4	1086.5
T7	4501.0	2442.5	−147.5	1315.1
T8	3874.6	3352.6	67.1	1013.8
T9	5447.6	3138.9	18.0	1445.7
T10	3656.9	3494.6	97.8	988.5
T11	4970.4	3086.4	−1.2	1341.4
T12	5181.3	2942.3	−21.2	1396.3

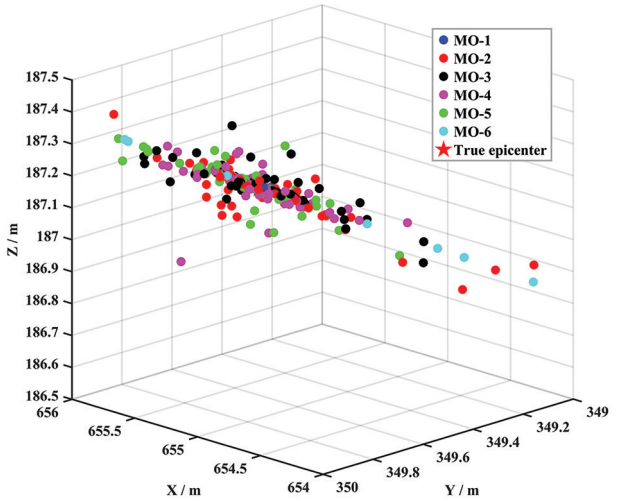

Figure 4. Local approximate dissolution point diagram of six microseismic source positioning combination models based on polyhedral array simulation and Multi-Objective Grasshopper Optimization Algorithm (MOGOA) model

Table 4. Statistical table of calculation results of six microseismic source positioning combination models based on the MOGOA model and deep mining microseismic events

Combination	Model 1	Model 2	Statistical values of microseismic source positioning results							
			Mean (m)	STD (m)	IQR (m)	Best (m)	Worst (m)	Duration (s)	Fit-1	Fit-2
MO-1	TDA	TDA-P1	768.4059	844.7945	981.4611	43.8738	3113.6014	4.8336	0.5187	6.3290
MO-2	TDA	TDQA	2815.2962	890.1189	152.6145	257.4626	3516.8166	8.4982	0.5766	0.0589
MO-3	TDA	TDQA-P1	1584.3049	1228.5779	2828.5199	42.3584	3102.2167	7.3851	0.5280	3.1257
MO-4	TDA-P1	TDQA	726.4571	1262.5554	139.1974	40.4096	3515.7592	7.9982	7.0129	0.0011
MO-5	TDA-P1	TDQA-P1	151.1915	66.5852	121.9566	41.0199	247.2754	7.5293	6.3129	1.3319
MO-6	TDQA	TDQA-P1	3509.2749	4.1603	7.9288	3503.0247	3516.7911	11.7089	0.0004	1.4036

Abbreviations: IQR: Interquartile range; MOGOA: Multi-Objective Grasshopper Optimization Algorithm; STD: Standard deviation; TDA: Time difference of arrival; TDQA: Time difference quotient of arrival.

limited by the large number of outliers identified by the box plot. The median and mean of its approximate solution set are second only to those of the MO-5 combination. It can be used as an alternative or substitute for the MO-5 combination model. The specific practical application effect needs to be further verified in combination with the second engineering blasting experiment.

(iii) From the perspective of fitness function value indicators (Fit-1, Fit-2), the statistical positioning effect of the combination MO-5 in the 100-round experiment is still possible to be improved. Its Fit-1 and Fit-2 values are 6.3129 and 1.3319, respectively. If the maximum number of iterations and the population size of the MOGOA algorithm are increased (such as 500 and 100), the positioning accuracy and robustness index values of the MO-5 combination model can be further improved. However, this will reduce the computational efficiency of the model and greatly increase the complexity of the process of finding the optimal approximate solution for the model. This is a practical problem that needs to be balanced in specific applications.

(iv) If the outliers (red triangles in Figure 5) divided by the box plot are ignored, the median and the 100-round positioning errors of the combination models MO-4 and MO-5 are very close. This shows that the MOGOA model, based on the MO-4 combination model, needs to add an outlier removal module to further improve the positioning accuracy and robustness of the results.

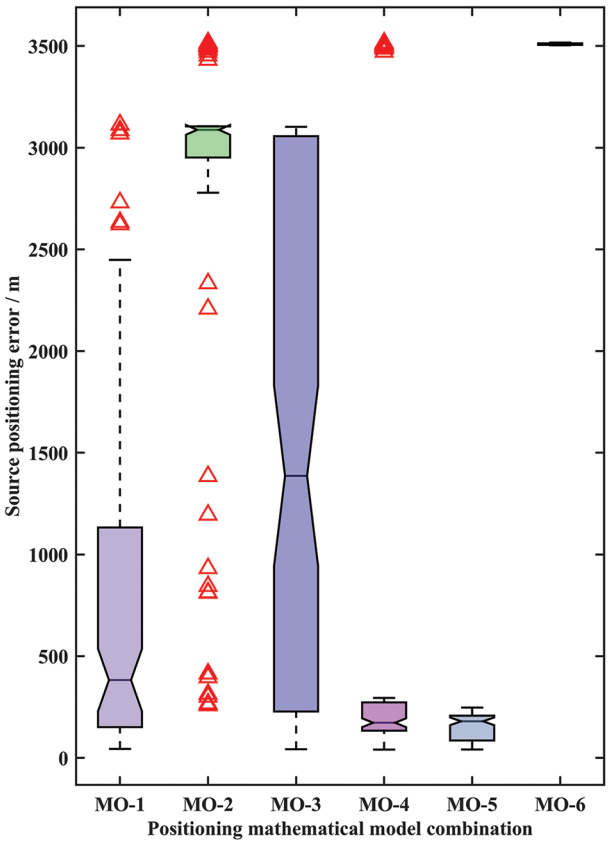

Figure 5. Box plot of calculation results based on Multi-Objective Grasshopper Optimization Algorithm (MOGOA) model and six combination models for microseismic source positioning under deep mining microseismic events

Figure 6 shows the curves of the calculation results of the six microseismic source positioning combination models based on the MOGOA model and deep mining microseismic events. Figure 7 shows the three-dimensional scatter plot of the calculation results of the MO-5 combination model based on the MOGOA model and deep mining microseismic events.

From Figures 6 and 7, we can see that:

(i) For a single combination model, the positioning result curves of the combination models MO-1 and MO-4 have a small number of sudden jumps, and are disturbed by a small number of large error positioning results and abnormal approximate solutions, resulting in a large overall positioning mean; while the 100-round positioning error curves of the other four combination models show a general oscillation phenomenon, which indicates that the original data of deep mining microseismic events used in this section may have large systematic errors from the first wave arrival time or the measurement point position coordinates, which makes the MOGOA optimization process unstable and prone to falling into local optimality.

(ii) As shown in Figure 7, the true source coordinates (3500.0, 3520.5, 102.0) are located outside the spatial coverage of the monitoring network. To a certain extent, this increases the difficulty of MOGOA in solving the source approximation solution. The positioning results of most model combinations all have high-frequency oscillation phenomena, which is consistent with the conclusion found by some researchers that the location effect of the internal source of the monitoring network is better than that of the external source.

Experiments on locating microseismic events in deep mining shafts analyzed the performance differences between MOGOA and multi-group multi-objective inversion models. However, varying microseismic event data quality and array configurations also impacted actual positioning effectiveness. We further incorporated microseismic events from the Shizhuyuan Mine for a second engineering case study, thereby strengthening the evaluation conclusions regarding the applicability of the core methodology presented herein.

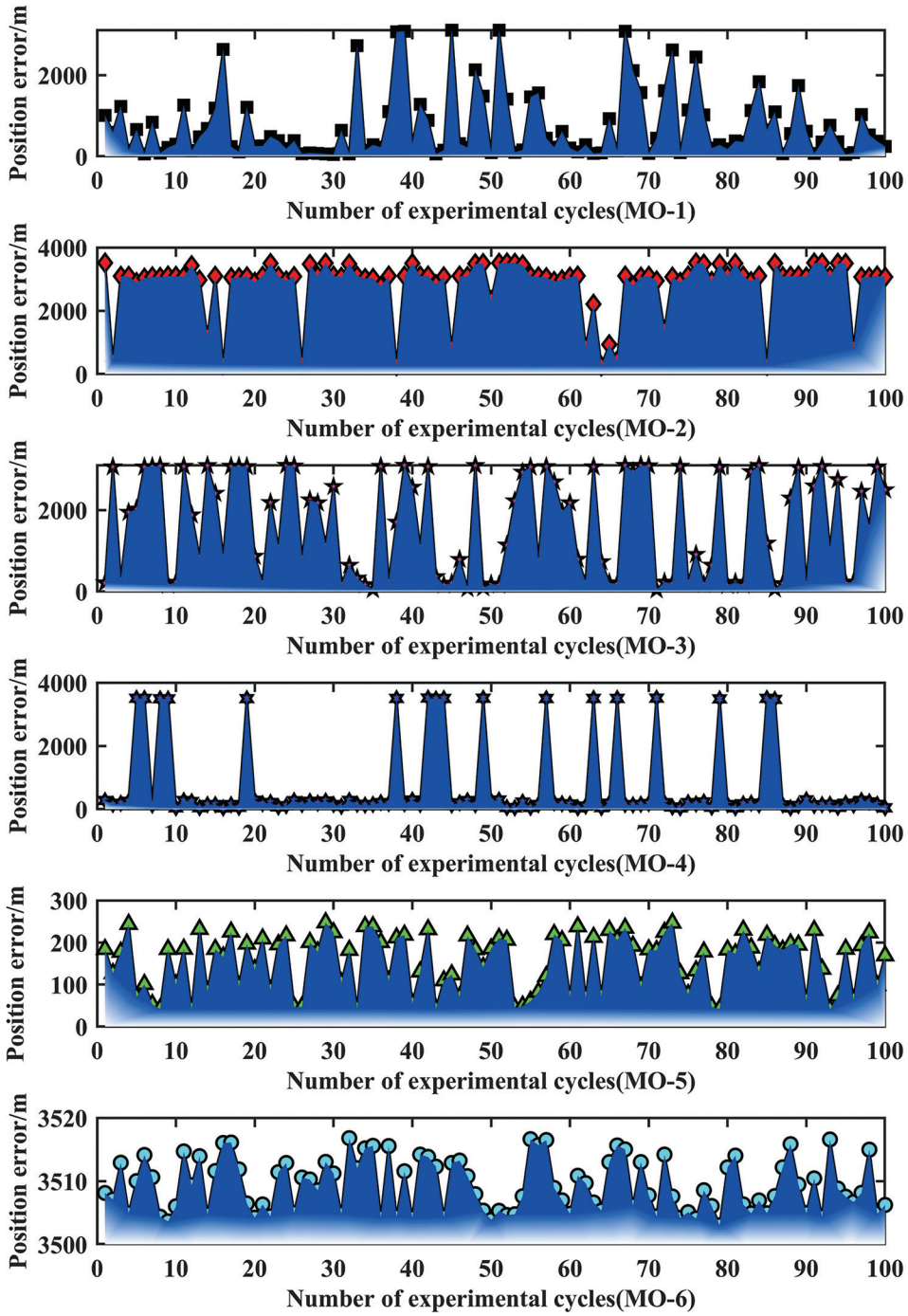

Figure 6. Position-error variations across 100 experimental cycles for six microseismic source positioning combination models (MO-1 to MO-6). All models are constructed using the Multi-Objective Grasshopper Optimization Algorithm (MOGOA) approach and tested with microseismic events from deep-mining environments.

5.2. Microseismic experiments at Shizhuyuan Mine in Hunan, China

To further verify the comprehensive positioning performance and application differences between the six microseismic source combination models and the MOGOA algorithm, we used microseismic data from the Shizhuyuan Mine in Hunan, China. The P-wave velocity was 2500 m/s, and the actual earthquake locations were (8732.70, 6570.60, 511.30). Eight seismic wave arrival times were recorded (Table 5). The results of 100 rounds

of microseismic source positioning experiments are shown in Figures 8–10 and Table 6. The MOGOA algorithm uses the following preset parameters: 40 search agents, 200 maximum iterations, 3 search target dimensions, a lower search limit of (5000, 5000, 0), an upper search limit of (10000, 10000, 1000), and 100 positioning experiment cycles.

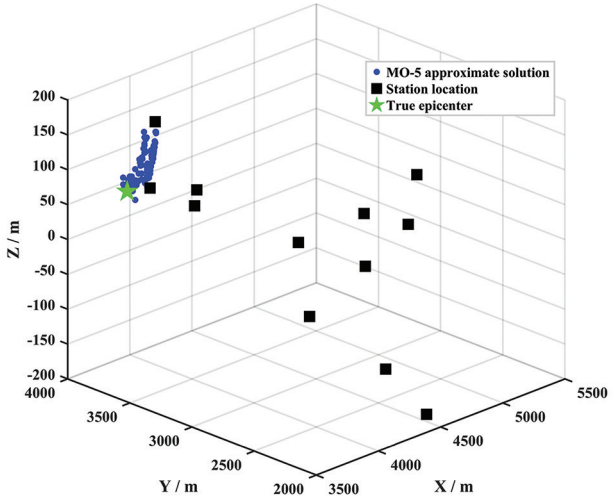

Figure 7. Three-dimensional scatter plot of calculation results based on Multi-Objective Grasshopper Optimization Algorithm (MOGOA) model and MO-5 combined model under microseismic events in deep mining

Table 5. Microseismic event data from a polymetallic mine in Shizhuyuan

Serial number	Detector	Vibration pickup coordinates (m)			By then (ms)
		x	*y*	*z*	
T1	9#	8761.00	6614.00	522.00	34.90
T2	21#	8737.00	6609.00	565.00	36.60
T3	5#	8666.00	6600.00	520.00	39.30
T4	17#	8668.00	6599.00	565.00	41.10
T5	4#	8641.00	6515.00	520.00	42.30
T6	8#	8691.00	6684.00	520.00	44.50
T7	2#	8721.00	6449.00	520.00	47.80
T8	26#	8702.00	6604.00	647.00	50.00

Table 6 shows the statistical results of the six combined models for microseismic source positioning based on the MOGOA model and the microseismic event occurring at Shizhuyuan Mine. The indicators Mean, IQR, STD, Best, Worst, Duration, Fit-1, and Fit-2 represent the mean, IQR, STD, minimum and maximum values of the location error dataset, the average calculated time for positioning, the final fitness function mean of Model 1 (the first submodel from the left in the combined model), and the final fitness function mean of Model 2, respectively. Figure 8 shows a box plot of the calculation results of six combined models for microseismic source positioning based on the MOGOA model and the microseismic event occurring at Shizhuyuan Mine. The upper and lower boundary lines of the boxes in the figure represent the upper quartile (Q3) and lower quartile (Q1) of the positioning results, respectively. The solid line inside the box represents the median of the positioning results. Red triangles mark data identified as outliers by boxplot. The upper and lower solid horizontal lines outside the box represent the maximum and minimum values, respectively.

From Figure 8 and Table 6, we can see that:

(i) In terms of positioning accuracy, the order is: MO-1 > MO-2 > MO-3 > MO-5 > MO-4 > MO-6. The positioning Mean value of the 100-round combination of the TDA and TDA-P1 models reached 27.6035 m, with the highest positioning accuracy. It also performed best in terms of the indicators IQR (5.5896 m) and STD (3.2114 m). This proves that the MO-1 combination has higher accuracy and a more robust model in the microseismic event occurring at Shizhuyuan Mine. The positioning results did not show excessive errors or were judged as outliers by the boxplot. Combined with the simulation experiments

Table 6. Calculation results of the six microseismic source positioning combination models based on the MOGOA model and microseismic event occurring at Shizhuyuan mine

Combination	Model 1	Model 2	Statistical values of microseismic source positioning results							
			Mean (m)	STD (m)	IQR (m)	Best (m)	Worst (m)	Duration (s)	Fit-1	Fit-2
MO-1	TDA	TDA-P1	27.6035	3.2114	5.5896	22.6275	34.8697	2.7545	0.0007	0.2166
MO-2	TDA	TDQA	67.8941	79.3381	80.4866	18.8058	571.4571	3.1671	0.0022	0.0098
MO-3	TDA	TDQA-P1	71.5070	89.5438	56.4096	15.2813	612.5145	3.1717	0.0025	0.4310
MO-4	TDA-P1	TDQA	261.6697	763.8916	100.3935	31.6485	3743.8654	3.2125	0.3539	0.0197
MO-5	TDA-P1	TDQA-P1	135.1657	347.8769	75.8264	29.9978	2547.7277	3.1662	0.3541	0.2354
MO-6	TDQA	TDQA-P1	2286.3621	1662.9977	3195.2378	146.7279	3743.2557	3.4758	3.2518e-05	0.1746

Abbreviation: MOGOA: Multi-Objective Grasshopper Optimization Algorithm.

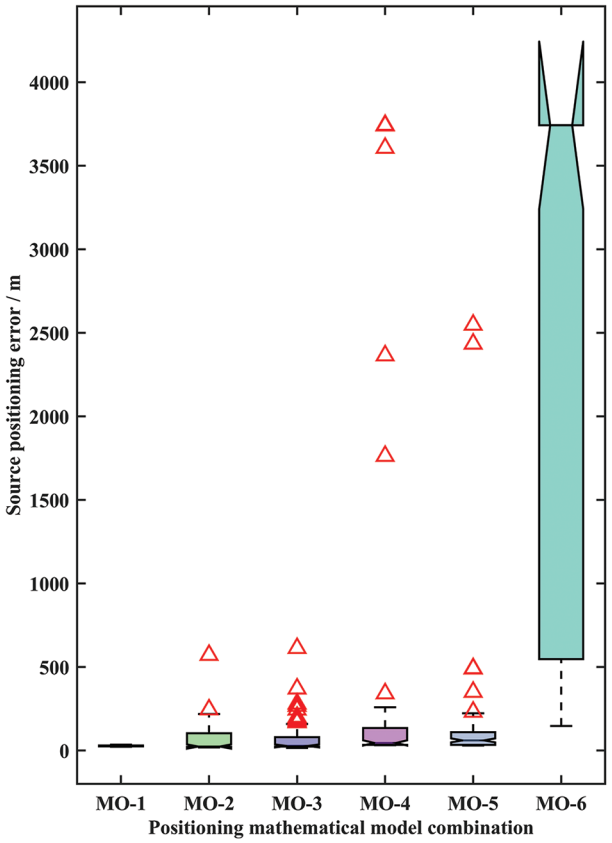

Figure 8. Box plot of calculation results based on Multi-Objective Grasshopper Optimization Algorithm (MOGOA) model and the six microseismic source positioning combination models for the microseismic event occurring at Shizhuyuan Mine, Hunan

in Section 3 and the engineering experiments in Section 4.1, we believe that the MO-1 combination is suitable for processing microseismic data with small errors in the position of microseismic array measurement points and small errors in the first wave arrival time.

(ii) The overall positioning accuracy and robustness of the MO-6 combination model are far inferior to those of other inversion mathematical models. In almost all evaluation indicators, it shows an abnormal state that is inconsistent with other combination models. Further analysis of the single mathematical model structure of the combination shows that since the combination does not use wave velocity as a parameter value of any fitness function of MOGOA, and the mathematical model in the form of quotient can only represent the relative positioning error, the combination model is more sensitive to the systematic error of the original data of microseismic events and is prone to fall into local optimality, which seriously restricts the global search ability of the optimization model.

(iii) As shown in Figure 8, if all the outliers filtered out by the box plot (marked as red triangles in Figure 8) are ignored, the median and mean of the 100-round positioning errors of MO-2, MO-3, MO-4, and MO-5 are almost the same. This provides us with an idea: based on MOGOA positioning, combining outlier elimination methods (such as the 3σ criterion, IQR method, and median absolute deviation method) will obtain a reliable approximate solution set.

Figure 9 shows the graphs of calculation results of the six microseismic source positioning combination models based on the MOGOA model and the microseismic event occurring at Shizhuyuan Mine. Figure 10 presents a three-dimensional scatter plot showing some of the calculation results of five microseismic source positioning combination models based on the MOGOA model and the microseismic event occurring at Shizhuyuan Mine.

From Figures 9 and 10, we can see that:

(i) For a single combination model, the positioning result curves of the MO-2, MO-3, MO-4, and MO-5 combination models only have a small number of curve jumps and some scattered points far away from the true source distribution, while the 100-round positioning error curve of MO-1 is relatively flat (all between 20 and 40 m). Combined with the statistical results in Section 4.1, it further shows that the microseismic data from the Shizhuyuan Mine used in this section contains less systematic errors and has little impact on the multi-round positioning effect.

(ii) MO-6 continues to have a large-scale curve jump phenomenon and a divergent distribution behavior far away from the true source, indicating that this model is not suitable for microseismic activity monitoring and related algorithm theory research.

To further elucidate positioning discrepancies among different combinations, we conducted nonparametric statistical tests on positioning error results (from 100 trials) across various model configurations. Given potential non-normal data distribution, we employed the Kruskal–Wallis *H* test, Dunn's post-hoc test (for multiple group comparisons), and Mann–Whitney *U* test (for two-group comparisons) to comprehensively assess statistically significant differences among combinations. Specific experimental details include:

(i) Kruskal–Wallis *H* test (multiple comparisons)
- Null hypothesis H0: The median positioning error is the same across all model combinations.
- Alternative hypothesis H1: At least one model combination has a different median positioning error.

(ii) Dunn's test (post-hoc multiple comparisons): Conducted only when the Kruskal–Wallis test is

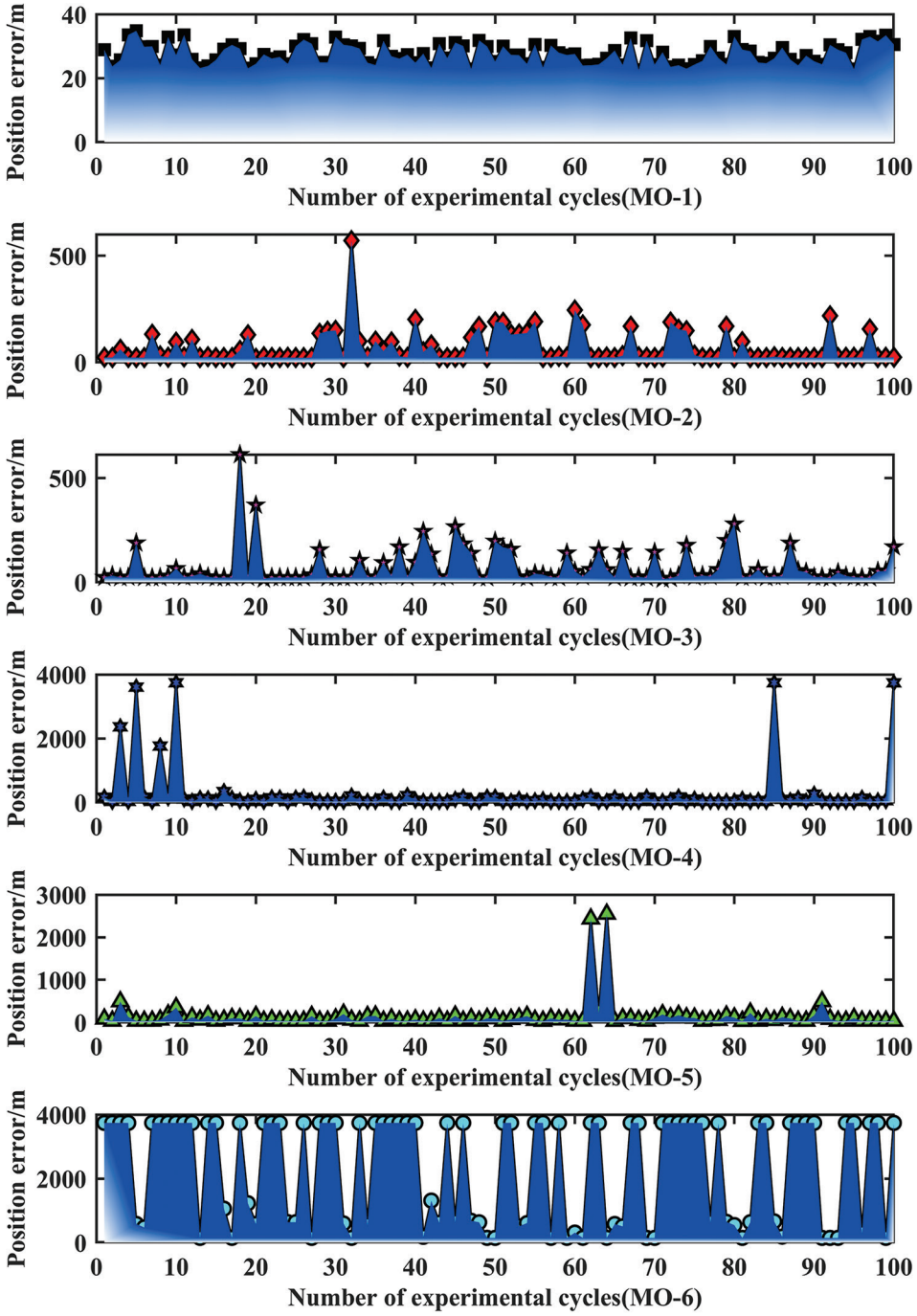

Figure 9. Graphs of calculation results based on Multi-Objective Grasshopper Optimization Algorithm (MOGOA) model and the six microseismic source positioning combination models for the microseismic event occurring at Shizhuyuan Mine, Hunan

significant, enabling pairwise comparisons among all combinations.

(iii) Mann–Whitney *U* test (key combination comparisons): Performed for pairwise comparisons of strongly complementary combinations expected to exhibit optimal performance. Selection criteria include comparisons between strongly complementary pairs and between strongly complementary and weakly complementary combinations.

The results of the nonparametric statistical test indicate the following: (i) The Kruskal–Wallis test yielded a p-value of 8.0472×10^{-68} and a mean of 323.6900. Since $p < 0.05$,

the null hypothesis is rejected, confirming that at least one combination exhibits a significant performance difference compared to the others. (ii) Post-hoc multiple comparisons (Dunn's test) results (as shown in Table 7): The p-values for MO-1 vs. MO-2, MO-1 vs. MO-3, MO-2 vs. MO-3, and MO-4 vs. MO-5 were 0.8120, 0.0783, 0.9853, and 1.0000, respectively, indicating no significant differences between the aforementioned paired combinations. (iii) In Mann–Whitney *U* test, comparisons of key combinations yielded p-values of 0.1039, 0.1045, 0, 0, and 0 for MO-2 vs. MO-3, MO-1 vs. MO-2, MO-2 vs. MO-6, MO-2 vs. MO-5, and MO-3 vs. MO-4, respectively. These indicate that no significant differences exist between MO-2 and MO-3 or MO-1, while MO-2 significantly outperformed MO-6 and MO-5, and MO-3 significantly outperformed MO-4. (iv) In summary, based on parameters such as the smallest coefficient of variation (0.1163) and the smallest mean positioning error (27.6035), the MO-1 combination demonstrates the best overall positioning performance.

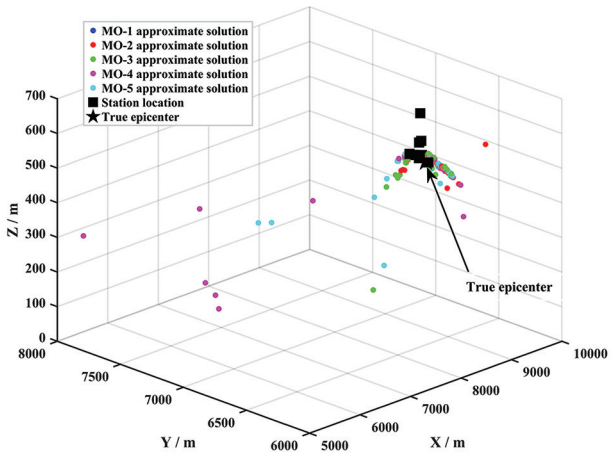

Figure 10. Three-dimensional scatter plot of partial results calculated based on Multi-Objective Grasshopper Optimization Algorithm (MOGOA) model and five types of microseismic source positioning combination models for the microseismic event occurring at Shizhuyuan Mine, Hunan

Table 7. Experimental results of Dunn's test based on microseismic source positioning results from Shizhuyuan Mine

Dunn's test	MO-1	MO-2	MO-3	MO-4	MO-5	MO-6
MO-1	1	0.8120	0.0783	0	0	0
MO-2	0.8120	1	0.9853	0	0	0
MO-3	0.0783	0.9853	1	0	0	0
MO-4	0	0	0	1	1.0000	0
MO-5	0	0	0	1.0000	1	0
MO-6	0	0	0	0	0	1

5.3. Comparative experiment on microseismic source positioning using MOGOA and similar multi-objective optimization algorithms

To verify the actual effect of MOGOA among similar multi-objective calculation methods, the microseismic event data of the Shizhuyuan Mine, which has a small systematic error in microseismic data, and the MO-1 combination with excellent positioning performance were uniformly used as experimental data and multi-objective optimization mathematical models for comparison of multi-objective optimization methods. The NSGA-II and the Multi-Objective Particle Swarm Optimization (MOPSO) were applied to compare and verify their positioning effects. Table 8 and Figure 11 show the microseismic source positioning results under the three multi-objective optimization models. The other experimental conditions were the same as the previous experiments: the number of swarm search agents was 40, the maximum number of iterations was 200, the search target dimension was 3, the search lower limit was (5000, 5000, 0), the search upper limit was (10000, 10000, 1000), and the number of positioning experiment cycles was 100.

Table 8 presents statistical results of microseismic source positioning after 100 iterations, compared with similar multi-objective optimization algorithms. Figure 11 shows a boxplot of microseismic source positioning results from three multi-objective optimization models based on the microseismic event occurring at Shizhuyuan Mine. Overall, the MOGOA method, compared to similar multi-objective calculation methods such as the NSGA-II method and the MOPSO method, exhibits significantly superior high-precision positioning (mean = 27.6035 m) and robust computational performance (STD = 3.2114 m), despite being inferior to the NSGA-II model in terms of algorithm computational efficiency (duration = 2.7545 s). It also balances the optimization processes of the two objective functions in the multi-objective optimization (Fit-1 and Fit-2 reach 0.0007 and 0.2166, respectively) and does not exhibit significant outliers that could severely restrict the practical application of the positioning algorithm. Therefore, it is a relatively reliable and effective microseismic source positioning method.

All experiments employed a population size of 40 and a maximum iteration count of 200 as the primary algorithmic parameters for MOGOA. The relationship between these parameter values and positioning performance has not been clearly elucidated. Therefore, in Section 4.4, we designed experiments specifically to analyze the impact of varying multi-objective algorithm parameters on positioning accuracy.

Table 8. Statistics of 100 rounds of microseismic source positioning results compared with similar multi-objective optimization algorithms

Multi-objective optimization methods	Model Portfolio	Statistical values of microseismic source positioning results							
		Mean (m)	STD (m)	IQR (m)	Best (m)	Worst (m)	Duration (s)	Fit-1	Fit-2
NSGA-II	MO-1	734.1109	552.4060	505.8955	27.2953	3.1833e+03	0.2874	0.0058	0.6619
MOPSO	MO-1	1.1892e+03	499.9879	524.0931	92.8176	4.1645e+03	3.3136	0.0058	0.6709
MOGOA	MO-1	27.6035	3.2114	5.5896	22.6275	34.8697	2.7545	0.0007	0.2166

Abbreviations: IQR: Interquartile range; MOGOA: Multi-Objective Grasshopper Optimization Algorithm; MOPSO: Multi-Objective Particle Swarm Optimization; NSGA-II: Second-generation nondominated sorting genetic algorithm; STD: Standard deviation.

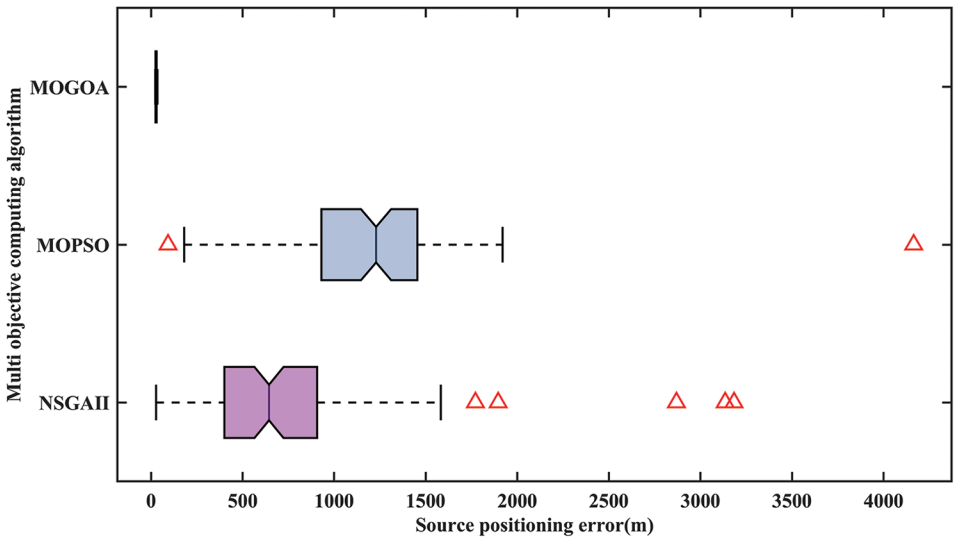

Figure 11. Box plot of three multi-objective optimization models for microseismic source positioning based on the microseismic event occurring at Shizhuyuan Mine, Hunan
Abbreviations: MOGOA: Multi-Objective Grasshopper Optimization Algorithm; MOPSO: Multi-Objective Particle Swarm Optimization; NSGA-II: Second-generation nondominated sorting genetic algorithm.

5.4. Sensitivity analysis of MOGOA parameters

Parameter sensitivity analysis is crucial for evaluating the robustness of positioning algorithms and guiding practical applications. To validate the sensitivity of MOGOA parameters (such as population size and maximum iteration count) on positioning performance, nine sets of microseismic source positioning experiments were designed with varying parameters. The Shizhuyuan Mine microseismic event data and the MO-1 ensemble were uniformly adopted as experimental data and the multi-objective optimization mathematical model for sensitivity analysis. Table 9 presents the statistical results of MOGOA microseismic source positioning under varying parameters. Other experimental conditions included: setting the number of agents in the population search to five levels (10, 20, 40, 80, 120); setting the maximum iteration count to five levels (20, 100, 200, 500, 1000); defining the lower search bound as (5000, 5000, 0) while the upper search bound as (10000, 10000, 1000); and setting the positioning experiment loop count to 20.

Our interpretations based on Table 9 are as follows: (i) With the maximum iteration count fixed at 200, parameter configurations exhibit distinct performance thresholds. When the population size is too small (population size = 10), the positioning error reaches as high as 859.6488 m, attributed to premature convergence caused by insufficient population diversity. However, when the population size exceeds 20, the positioning error stabilizes around 31 m, indicating that a critical level of diversity has been achieved to ensure algorithmic performance. (ii) Similarly, with the population size fixed at 40, when the maximum iterations were below 100 (maximum iterations = 50), the algorithm performed poorly (error 134.3802 m) due to insufficient convergence time; performance stabilized when iterations exceeded 100. (iii) These findings demonstrate the proposed method's robust parameter tolerance. Stable and accurate positioning

Table 9. Statistical table of microseismic source positioning for MOGOA under different parameters

Population size	Maximum iterations	Statistical values of microseismic source positioning results						
		Mean (m)	STD (m)	IQR (m)	Best (m)	Worst (m)	Duration (s)	Median (m)
10	200	859.6488	1.0750e+03	1.2744e+03	28.1846	3.4119e+03	0.3577	256.4745
20	200	31.4368	2.2932	3.4162	27.9417	35.8210	0.7592	30.6503
40	200	31.0989	2.0841	3.5635	28.6328	34.9410	2.8058	30.4776
80	200	31.7041	2.4019	4.4000	28.0602	35.2399	10.9193	31.5326
120	200	30.9992	2.1564	2.7094	28.3879	36.7719	24.4511	30.3021
40	50	134.3802	180.4892	175.2767	28.6574	641.0793	0.7172	35.0223
40	100	43.5813	52.3692	4.1199	27.4581	265.7581	1.3974	31.3012
40	500	31.1093	2.3525	4.3755	28.3230	35.1322	7.0539	30.1602
40	1000	32.3111	2.0417	3.6189	29.0395	34.6590	14.1781	33.2069

Abbreviations: IQR: Interquartile range; MOGOA: Multi-Objective Grasshopper Optimization Algorithm; STD: Standard deviation.

results are achievable as long as parameter configurations exceed the minimum thresholds (population size ≥20, maximum iterations ≥100). Based on this, population size = 40 and maximum iterations = 200 were selected as experimental parameters, balancing performance assurance with computational efficiency.

6. Conclusion

This paper uses the MOGOA model to examine the performance differences among six microseismic source positioning mathematical model combinations and validates the application and adaptability of the inversion model combination to three types of microseismic event data. The performance of MOGOA is then compared with that of NSGA-II and MOPSO for a similar location. The following conclusions are drawn:

(i) When microseismic event data errors are minimal, the MO-1 combination, consisting of the TDA-P1 and TDA models, exhibits superior microseismic source positioning performance, demonstrating significant performance in positioning accuracy, robustness, and computational efficiency. Applying a multi-objective intelligent swarm optimization algorithm to the microseismic source positioning mathematical model effectively adds constraints to the nonlinear problem, effectively preventing the optimization process from prematurely falling into local optima. The MOGOA and MO-1 model combination is suitable for processing data from sites with precise array sensor positions and relatively uniform surface media.

(ii) When microseismic event data errors are large, the MO-5 combination, consisting of the TDA-P1 and TDQA-P1 models with a constant offset term, achieves superior microseismic source positioning performance. The TDQA-P1 model mathematically eliminates wave velocity and first wave arrival time, further reducing the impact of these parameter errors on location. Therefore, the MOGOA and MO-5 combination is suitable for processing data from sites with errors in array sensor positions or inhomogeneous surface media.

(iii) Compared with similar multi-objective algorithms such as NSGA-II and MOPSO, MOGOA exhibits significant noise immunity and global search capabilities, and can be further analyzed and applied in research on optimal microseismic source positioning based on inversion mathematical models.

(iv) Parameter sensitivity analysis reveals that the proposed combination of inversion models provides an effective search space for the optimization algorithm, enabling the multi-objective ant colony algorithm to converge stably under relatively relaxed parameter settings. This facilitates the practical application of this method in engineering practice.

(v) This study confirms that determining microseismic source location is a multi-objective optimization problem and intelligent algorithms provide a robust strategy to microseismic source positioning. This approach does not rely on a single, potentially inaccurate assumption—whether concerning the velocity model or data quality. Instead, it naturally derives an optimal compromise solution insensitive to various errors through the synergistic and competitive interaction of multiple models. This endows it with clear application potential and advantages over traditional methods in real-world engineering scenarios where model and data uncertainties exist.

In future research, we will focus on addressing the challenges of low positioning accuracy and poor model robustness caused by systematic errors in microseismic event data. We plan to introduce an adaptive step-size adjustment mechanism in the MOGOA model, linked to the fitness function value or the number of iterations,

to enhance MOGOA's global search capabilities in inhomogeneous media.

Acknowledgments

None.

Funding

This research was financially supported by Mahasarakham University; the Scientific Research Fund from Institute of Seismology, CEA and National Institute of Natural Hazards, Ministry of Emergency Management of China (Grant No. IS202226322 and IS202436357); the Open Fund of Wuhan Gravitation and Solid Earth Tides, National Observation and Research Station (Grant No. WHYWZ202406); the Spark Program of Earthquake Science and Technology, China Earthquake Administration (Grant No. XH25019C and XH24025YC); the 2025 Hubei Provincial Key Laboratory Targeted Commissioned Project (Grant No. 2025CSA083); the Green Data Integration Intelligence Research and Innovation Project of Chengdu Jincheng College (Grant No. 2025–2027); and the Mathematics and Finance Research Center Project of Dazhou Social Science Federation Key Research Base (Grant No. SCMF202505).

Conflict of interest

The authors declare they have no competing interests.

Author contributions

Conceptualization: Cong Pang, Tianwen Zhao, Sirui Liu, Xingxing Li, Ya Xiang

Formal analysis: Cong Pang, Guoqing Chen, Tianwen Zhao, Ya Xiang

Investigation: Tianwen Zhao, Sirui Liu, Xingxing Li, Piyapatr Busababodhin

Methodology: Cong Pang, Tianwen Zhao, Guoqing Chen, Piyapatr Busababodhin

Validation: Cong Pang, Shirui Liu, Tianwen Zhao, Guoqing Chen

Writing–original draft: Cong Pang, Tianwen Zhao, Guoqing Chen, Piyapatr Busababodhin

Writing–review & editing: Cong Pang, Tianwen Zhao, Guoqing Chen, Piyapatr Busababodhin

Availability of data

Some data used in this study cannot be shared publicly due to collaborative agreement restrictions but are available from the corresponding author upon reasonable request.

References

1. Feng Q, Han L, Ma L. Microseismic source localization method based on neural network algorithm and dynamic reduction of solution interval. *IEEE Geosci Remote Sens Lett*. 2024;21:1-5.

   doi: 10.1109/lgrs.2024.3398043

2. Yan Z, Zi-Zin W, Lin-Qi C, Hong-Li D. Research on microseismic event localization based on convolutional neural network. *J Seismic Explor*. 2024;33(6):1-32.

   doi: 10.36922/jse.corr090325

3. Wang H, Alkhalifah T, Waheed UB, Birnie C. Data-driven microseismic event localization: An application to the Oklahoma Arkoma basin hydraulic fracturing data. *IEEE Trans Geosci Remote Sens*. 2022;60:1-12.

   doi: 10.1109/TGRS.2021.3120546

4. Feng Q, Han L, Zhao B. Localizing microseismic events using semi-supervised generative adversarial networks. *IEEE Trans Geosci Remote Sens*. 2022;60:5923908.

   doi: 10.1109/tgrs.2022.3225415

5. Xu J, Qiu T, Zeng Z, Zhu F, Han P, Zhang W. Microseismic event location using migration-based stacking with effective parameters' optimization. *IEEE Trans Geosci Remote Sens*. 2025;63:5917809.

   doi: 10.1109/tgrs.2025.3591126

6. Chen Y, Savvaidis A, Fomel S, Saad OM, Chen Y. RFloc3D: A machine-learning method for 3-D microseismic source location using P- and S-wave arrivals. *IEEE Trans Geosci Remote Sens*. 2023;61:1-10.

   doi: 10.1109/tgrs.2023.3236572

7. Michel OJ, Tsvankin I. Gradient calculation for waveform inversion of microseismic data in VTI media. *J Seismic Explor*. 2014;23(3):201-217.

8. Abdullin A, Waheed UB, Suleymanli K, Stanek F. Microseismic source localization using fourier neural operator with application to field data from Utah FORGE. *IEEE Trans Geosci Remote Sens*. 2025;63:1-10.

   doi: 10.1109/tgrs.2025.3533635

9. Wang C, He R, Pei C, Sun F, Zhou X, Chen Z. Localization for surface microseismic monitoring based on local equivalent path and virtual field optimization method. *IEEE Sens J*. 2024;24(23):39270-39284.

   doi: 10.1109/jsen.2024.3469969

10. Pang C, Xu J, He X, Zuo Y, Li C, Ma W. Research on Location Method of Mine Micro-Seismic Source Based on Inter Quartile Range and Newton-Raphson Method. In: *2023 International Conference on New Trends in Computational Intelligence (NTCI)*. Qingdao, China; 2023. p. 5-10.

    doi: 10.1109/ntci60157.2023.10403666

11. Pang C, Chen J, Ma L, *et al*. A Method for Micro-seismic Source Location Based on Principal Component Analysis and Spatial Discrete Detection. In: *2023 IEEE 7th Information*

Technology and Mechatronics Engineering Conference (ITOEC). Chongqing, China; 2023. p. 92-96.

doi: 10.1109/itoec57671.2023.10291402

12. Wang Y, Bi W, Fan Q, Xu S, Zhang A. Multi-objective optimization of top-level arrangement for flight test. *J Syst Eng Electron*. 2025;36(3):714-724.

doi: 10.23919/jsee.2025.000019

13. Noori MS, Sahbudin RKZ, Sali A, Hashim F. Multi-objective multi-exemplar particle swarm optimization algorithm with local awareness. *IEEE Access*. 2024;12:125809-125834.

doi: 10.1109/access.2024.3426104

14. Gao L, Liu Z. An integrated external archive local disturbance mechanism for multi-objective snake optimizer. *Chin J Electron*. 2024;33(4):989-996.

doi: 10.23919/cje.2023.00.023

15. Sadeghi AH, Bani EA, Fallahi A, Handfield R. Grey wolf optimizer and whale optimization algorithm for stochastic inventory management of reusable products in a two-level supply chain. *IEEE Access*. 2023;11:40278-40297.

doi: 10.1109/access.2023.3269292

16. Wu X, Zhan J, Ding W, Pedrycz W. GRNN model with feedback mechanism incorporating *k*-nearest neighbor and modified gray wolf optimization algorithm in intelligent transportation. *IEEE Trans Intell Transp Syst*. 2025;26(3):3855-3872.

doi: 10.1109/tits.2024.3510678

17. Chen X, Ma M, Liu C, Xie H, Wang S. Research on interference resource optimization based on improved whale optimization algorithm. *IEEE Access*. 2025;13:83136-83147.

doi: 10.1109/access.2025.3569460

18. Zhao ZH, Yin YF, Wang YK, Qin KR, Xue CD. Adaptive ECG signal denoising algorithm based on the improved whale optimization algorithm. *IEEE Sens J*. 2024;24(21):34788-34797.

doi: 10.1109/jsen.2024.3422995

19. Li Y, Yao Y, Hu S, Wen Q, Zhao F. Coverage enhancement strategy for WSNs based on multiobjective ant lion optimizer. *IEEE Sens J*. 2023;23(12):13762-13773.

doi: 10.1109/jsen.2023.3267459

20. Tian F, Zhu L, Shi Q, *et al*. The three-lead EEG sensor: Introducing an EEG-assisted depression diagnosis system based on ant lion optimization. *IEEE Trans Biomed Circ Syst*. 2023;17(6):1305-1318.

doi: 10.1109/tbcas.2023.3292237

21. Ghaleb SA, Mohamad M, Ghanem WAH, *et al*. Feature selection by multiobjective optimization: Application to spam detection system by neural networks and grasshopper optimization algorithm. *IEEE Access*. 2022;10:98475-98489.

doi: 10.1109/access.2022.3204593

22. Liu J, Wang A, Qu Y, Wang W. Coordinated operation of multi-integrated energy system based on linear weighted sum and grasshopper optimization algorithm. *IEEE Access*. 2017;6:42186-42195.

doi: 10.1109/access.2018.2859816

23. Lalhmachhuana R, Deb S, Datta S, Singh KR. Multi-Objective based Generation Fuel Cost and Emission Reduction using Grasshopper Optimization Algorithm. In: *2023 10th International Conference on Signal Processing and Integrated Networks (SPIN)*. Noida, India; 2023. p. 676-680.

doi: 10.1109/spin57001.2023.10116665

24. Mokeddem D, Nasri D. A New Levy Flight Trajectory-based Grasshopper Optimization Algorithm for Multi-Objective Optimization Problems. In: *2020 Second International Conference on Embedded and Distributed Systems (EDiS)*. Oran, Algeria; 2020. p. 76-81.

doi: 10.1109/edis49545.2020.9296480

25. Zhaoming LV, Peng R. Improving the efficiency of multi-objective grasshopper optimization algorithm to enhance ontology alignment. *Wuhan Univ J Nat Sci*. 2022;27(3):240-254.

doi: 10.1051/wujns/2022273240

26. Wang C, Li J, Rao H, *et al*. Multi-objective grasshopper optimization algorithm based on multi-group and co-evolution. *Math Biosci Eng MBE*. 2021;18(3):2527-2561.

doi: 10.3934/mbe.2021129

27. Pang C, Zhao T, Chen G, *et al*. Earthquake and blast recognition based on CEEMDAN multiscale fuzzy entropy and NSGAIII optimized 1D-CNN neural networks. *J Seismic Explor*. 2025;34(1):22-42.

doi: 10.36922/jse025260029

28. Bahrami B, Khayyambashi MR, Mirjalili S. Multiobjective placement of edge servers in MEC environment using a hybrid algorithm based on NSGA-II and MOPSO. *IEEE Int Things J*. 2024;11(18):29819-29837.

doi: 10.1109/jiot.2024.3409569

29. Li Y, Xie Z, Yang S, Ren Z. A hybrid algorithm based on NSGA-II and MOPSO for multi-objective designs of electromagnetic devices. *IEEE Trans Magn*. 2023;59(5):7001804.

doi: 10.1109/tmag.2023.3250319

30. Poormirzaei R, Hamidzadeh R, Moghadam R, Zarean A. The application of PSO to joint inversion of microtremor Rayleigh waves dispersion curves and refraction traveltimes. *J Seismic Explor*. 2015;24(4):305-325.